EXTENDING AND TESTING GRAIZER-KALKAN GROUND MOTION ATTENUATION MODEL BASED ON ATLAS DATABASE OF SHALLOW CRUSTAL EVENTS

Vladimir Graizer[1], Erol Kalkan[2] and Kuo-Wan Lin[3]

ABSTRACT

A new ground motion prediction equation (GMPE) based on representation of attenuation function as a series of filters has been developed using expanded NGA database (Graizer and Kalkan 2007). In this GMPE, each filter represents a certain physical phenomenon on seismic radiation (e.g., distance attenuation, magnitude scaling, site-correction, basin effect, etc.). We use moment magnitude (denoted as M_w or M) and closest distance to the fault (denoted as R_{cl} or R) in our model. The predictive power of this GMPE is examined using a comprehensive set of peak ground acceleration (PGA) data (~14,000) compiled from 245 worldwide shallow crustal events. Comparison of actual data with predictions demonstrates a very good match up to 100 km for a range of magnitudes $4.2 \leq M_w \leq 7.9$. In order to model a faster attenuation of ground motion data beyond 100 km, two estimator coefficients are updated and a new filter is implemented. The resultant GMPE GK-09 produces good match to recorded global data in both near- and far-field up to 500 km.

Introduction

In many seismic regions, there is not enough recorded ground motion data from a wide range of magnitudes to develop regional GMPEs. For seismic hazard studies in these regions it is customary to import GMPEs originally developed using ground motion data from other tectonic environments. For instance, 97 era GMPEs (e.g., Boore et al. 1997; Campbell 1997) developed based on Western U.S. (WUS) ground motions have found widespread use in shallow crustal regions much beyond their original range of magnitude and distances. The Next Generation of Attenuation (NGA) database has provided more complete source of ground motions compiled from active tectonic regions similar to the WUS. This database has over 3000 data points; more than 500 are from the 1999 Chi-Chi (Taiwan) earthquake and the majority of the rest are from the Californian events (Power et al. 2006). The NGA database with a number of additions (e.g., 2003 San Simeon and 2004 Parkfield earthquakes in California) was used to develop the GK-07

[1] U.S. Nuclear Regulatory Commission, Washington, DC 20555, Vladimir.Graizer@nrc.gov
[2] U.S. Geological Survey, 345 Middlefield Rd., Menlo Park, CA 94025, ekalkan@usgs.gov
[3] U.S. Geological Survey, Denver, CO, 80225 klin@usgs.gov

GMPE (Graizer and Kalkan 2007). The GK-07 predicts well the ground motions recorded not only from the Californian events, but also Denali (Alaska), Chi-Chi, Kocaeli and Dűzce (Turkey) earthquakes.

The GK-07 models attenuation function as a combination of filters where each filter represents a certain physical phenomenon on seismic radiation (e.g., magnitude scaling, site-correction, basin effect, etc.). This approach provides an enhanced robustness and stability to a GMPE by separating influence of each phenomenon on ground motion attenuation. In this paper, the performance of the GK-07 in predicting PGA in near- and far-field up to 500 km is examined using a comprehensive set of data. Ground motion prediction at distances more than 200 km (beyond the range of the NGA database) has a particular interest for the nuclear industry and seismic hazard mapping in stable continental regions.

GMPE is a key part of ShakeMap development. ShakeMap is now a well-known product and is widely used all around the world including the regions were there are no or not enough strong motion data collected to create regional attenuation. In this case using the "global" attenuation relationship may be better than simply importing GMPE developed for another tectonic environment.

Ground Motion Database

USGS – Atlas global database (http://earthquake.usgs.gov/eqcenter/shakemap/atlas.php) was used to compile 13,992 PGA data from 245 worldwide shallow crustal events. The compiled database includes PGA (>0.001g) recorded within 500 km of fault rupture from earthquakes having magnitude range 4.2 - 7.9. The distributions of PGA data against moment magnitude M_W (denoted M), closest distance to the fault R_{cl} (denoted R) and shear wave velocity in the upper 30 m V_{S30} are shown in Fig. 1; also shown is the extended NGA database utilized for the GK-07. As evident, new dataset is more complete not only at far-field but also at near-field; it is also more inclusive in terms of geological conditions and magnitude range covered. The latest entities are the 2008 M_W7.9 Wenchuan (China) and the 2009 M_W6.3 L'Aquila (Italy) earthquakes.

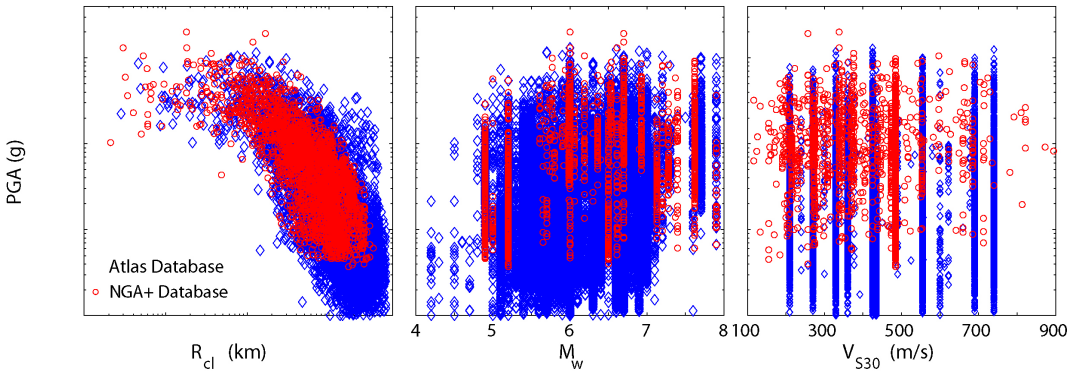

Figure 1. Distribution of PGA values with respect to moment magnitude (M_W), closest distance to the fault (R_{cl}), and shear-wave velocity (V_{S30}).

Graizer-Kalkan Ground Motion Prediction Model

According to Campbell (2003) an attenuation relation in its most fundamental form can be described by the following ground motion (*GM*) prediction equation:

$$\ln(GM) = c_1 + c_2 M - c_3 \ln R + c_4 R + c_5 F + c_6 S + \sigma \tag{1}$$

where M is a magnitude, R is a distance, F is a parameter characterizing style of faulting, S is a parameter characterizing the local site condition, σ is a random error term with zero mean (i.e., normally distributed). Most GMPE developers are using an approach based on Eq. (1), e.g., Abrahamson and Silva, Boore and Atkinson, Campbell and Bozorgnia, Chiou and Youngs, Idriss (2008). Since ground motion data is considered to be lognormally-distributed, an advantage of using Eq. (1) is to simplify data-fitting through regression by linearization. On the other hand, it pushes researchers to search for a fixed functional form between logarithm of ground motion parameter (e.g., PGA) and magnitude, distance and other independent parameters suitable for both near- and far-field. This may result in very complex dependencies, such as square of magnitude (Boore and Atkinson 2008) or hyperbolic cosine function (Chiou and Youngs 2008). In addition, Eq. (1) assumes an exponential approximation of ground motion attenuation, a restricted type of representation not necessary supported by theory and empirical data. According to the wave propagation theory, residual displacements attenuate as R^{-2}, *P*- and *S*-waves attenuate as R^{-1} and surface waves attenuate as $R^{-0.5}$, meaning that ground motion attenuation theoretically follows a power law. Let us look how ground motion recorded from earthquakes attenuates in near-field; spatial distribution of ground motion data recorded in the proximity of earthquake fault zones (e.g., Mogul 2008, Parkfield 2004, Chi-Chi 1999, Northridge 1994, Loma Prieta 1989 and Imperial Valley 1979) revealed important attenuation characteristics of PGA as:

(1) Remains constant in near-field (flat response – no attenuation),
(2) Exhibits an increase in amplitude (bump on attenuation curve) or a turning point at certain distances (about 3-10 km from the fault rupture),
(3) Attenuates with a slope of R^{-1} and faster at far distances (R > 10 km),
(4) Its amplitude amplifies at certain distances due to basin effect or reflection from the Moho surface,
(5) Depending upon crustal characteristics, it can attenuate much faster at large distances (R > 100 km) due to regional low Q-values as in the WUS in comparison with the CEUS.

As shown in Graizer and Kalkan 2007, the 2004 M_W6.0 Parkfield earthquake presents an excellent case of a well recorded event at near- and far-field. It is evident that an exponential attenuation curve with a constant attenuation rate could not be a best fit to recorded data. The attenuation characteristic of the Parkfield data is similar to frequency response function of a SDF oscillator: flat response at the beginning, possible bump and a turning point, and sharp decay. As was shown by Graizer and Kalkan (2007) substituting square of frequency (ω^2) term with distance (R) term in the SDF formula, we obtain the core attenuation equation as:

$$G\,(M, R, C_0) = 1 \Big/ \sqrt{\left[1 - (R/R_0)\right]^2 + 4D_0^2 (R/R_0)} \tag{2}$$

where D_0 is a damping term.

We also suggest using the following mathematical formulation instead of Eq. (1) to represent the GMPE:

$$PGA = G_1(M,F)\cdot G_2(M,R,C_2)\cdot G_3(M,R,C_3)\cdot G_4(M,C_4)\cdot G_5(M,R,C_5)\cdot \sigma_{PGA} \quad (3)$$

In this representation each function (G_n) is in multiplication form (cascade of filters) helping to better understand their influence on resultant ground motion intensity. Eq. 3 may be expressed in logarithmic space as:

$$\ln(PGA) = \sum_n \ln[G_n(M,R,C_n,F)] + \sigma_{\ln PGA} \quad (4)$$

Using separate functions (G_n) in GMPE and modeling ground motion attenuation by means of a SDF response function provide a number of advantages:

1. It allows representing each physical phenomenon on seismic radiation by a separate filter as a function of independent physical parameters (e.g., *M*, *R*).
2. Instead of fitting an empirical equation to entire dataset via single or two-stage regression, filter-based approach allows for sequential data fitting and robust nonlinear optimization.
3. It eliminates the need to search for a complex and purely empirical equation form.

In Eq. (3, 4), the first filter, G_1, is for magnitude and style of faulting scaling, G_2 (also called as "core attenuation equation") models attenuation of ground motion in near- and intermediate-field. G_3 represents intermediate distance correction and basin effect. G_4 is for ground motion amplification due to shallow site conditions, and G_5 adjusts the slope of attenuation curve at far distances. Amplification of ground motion due to reflections from Moho surface, near-field directivity and hanging wall effects can also be represented by separate filters.

Except G_4, each filter utilized is a linear or nonlinear function of at least *M* and *R*. G_2, G_3 and G_5 have a corner distance parameter, defining either the distance after which the filter is effective or at which the maximum amplification (bump) associated with this filter takes place. For completeness, each filter is briefly explained in the following:

Filter G_1: Magnitude and Style of Faulting Scaling

The following scaling function is utilized to model magnitude and style of faulting scaling:

$$G_1(M,F) = [c_1 \arctan(M + c_2) + c_3]F \quad (5)$$

where c_1, c_2 and c_3 are estimator coefficients, and *F* represents scaling due to style of faulting. This scaling function reflects saturation of amplitudes of ground motion with increasing magnitudes. $F = 1.00$ for strike-slip and normal faults, and $F = 1.28$ for reverse faults.

Filter G_2: Core Attenuation Equation

In the GK-07, the corner distance and damping in the core equation were R_0 and D_0. For consistency with G_2 we refer them R_2 and D_2 in Eq. (6). R_2 is a function of *M* and D_2 quantifies the intensity of bump on the attenuation curve.

$$G_2(M,R,C_2) = 1\Big/\sqrt{\left[1-(R/R_2)\right]^2 + 4D_2^2(R/R_2)}$$

$$R_2 = c_4 M + c_5 \qquad D_2 = c_6 \cos(c_7 M + c_8) + c_9 \tag{6}$$

where c_4, c_5, c_6, c_7, c_8 and c_9 are estimator coefficients. Eq. (6) implies that for larger magnitudes, turning point on attenuation curve occurs at larger distances. D_2 is a function of magnitude reaching minimum with $D_2 = 0.4$ (producing a significant bump) for the range M6.0 – 6.5 and being higher at M<5.0 and M>7.0 (much lower or no bump). Relative level of bump on attenuation curve decreases for larger and smaller magnitudes; recorded data shows that for M>7.5, bump saturates.

Filter G_3: Sediment Depth Basin Effect

Basin effect significantly impacts wave field at distances 30-50 km and more when deep sedimentary basin is present (Lee et al., 1995; Campbell, 1997). In most cases it creates large amplitude surface waves. We model this effect by applying the G_3 filter. Similar to G_2, G_3 filter is determined by two parameters: distance, R_3 and damping, D_3. R_3 describes the distance for bump on the attenuation curve (amplification due to basin), and D_3 describes its amplitude (lower value of D_3 produces higher amplitudes of bump). If sediment thickness is low, basin effect can be neglected and D_3 can be taken as 0.65 - 0.70 (no bump). G_3 filter with this value of D_3 results in a change of slope on attenuation curve at distances larger than R_3 only; it remains ineffective for distances less than R_3. which is fixed at 100 km. Resultant attenuation function $(G_2 \cdot G_3)$ decays proportionally to $R^{-1.5}$ at distances $R >> R_3$ unlike R^{-1} decay produced by G_2 filter.

We envision damping parameter of the G_3 filter (D_3) to be a smooth function of basin depth. As a first approximation, we simply consider basin effect to be same for all sediment depths (Z) more than 1 km.

$$G_3(M,R,C_3) = 1\Big/\sqrt{\left[1-(R/R_3)^{0.5}\right]^2 + 4D_3^2(R/R_3)^{0.5}}$$

$$D_3 = \begin{cases} 0.65 \text{ for } Z < 1 \text{ km} \\ 0.35 \text{ for } Z \geq 1 \text{ km} \end{cases} \tag{7}$$

D_3 is expected to decrease smoothly from 0.7 to 0.3-0.4 and saturate with an increase in sediment thickness.

Filter G_4: Effect of Shallow Site Conditions

Cross-comparison of NGA GMPEs demonstrates significant differences in site amplification for PGA and spectral acceleration ordinates for soft-soils (V_{S30} < 400 m/sec) (2009 SSA presentation of Prof. I.M. Idriss). These differences call for further calibration of nonlinear models using experimental data. Following Boore et al. (1997) we adopt linear site amplification that can be formulated in natural logarithmic space as:

$$ln(G_4) = b_v \cdot ln(V_{S30}/V_A) \tag{8}$$

Similar to Field (2000), our attenuation model exhibits less amplification ($b_v = -0.24$ instead of -0.371) as the V_{S30} decreases compared to Boore et al. 1997.

Filter G_5: Far Distance Attenuation Filter

For distances more than 100 km from a fault (increasing with the increase of M) attenuation of ground motion data demonstrate two main tendencies: Faster attenuation in the order of R^{-4}, and slower attenuation in the order of $R^{-1.5}$. Increase in the attenuation slope i.e., faster attenuation is due to relatively low Q-values and slower attenuation is due to high Q-values. For regions similar to the Central and Eastern U.S. with relatively high Q-values (Singh and Herrmann 1983; Mitchell and Hwang 1987), attenuation at far-field is about the same as in near-field (about $R^{-1.5}$). In the WUS and other active tectonic regions with relatively low Q-values, attenuation is faster (almost R^{-4}) at far distances (e.g., 2004 Parkfield earthquake).

To model fast attenuation at far distances, the following filter is used:

$$G_5(M,R) = 1\Big/\sqrt{\left[1-(R/R_5)^d\right]^2 + 4D_5^2(R/R_5)^d} \tag{9}$$

G_5 has a flat region at distances $R<R_5$, a turning point around the corner distance, R_5, for damping parameter, D_5 = 0.6-0.7. The slope of attenuation curve is determined by an adjustable parameter d, varying from 0 to 2.5; 0 means no adjustment to attenuation slope. For the Atlas dataset which constitutes a mixture of data from different tectonic regions, an average value of $d=0.5$ is used. In Eq. 9 R_5 increases with magnitude, $R_5 = c_{11}M^2 + c_{12}M + c_{13}$. Use of G_5 brings final attenuation slope at far distances to $R^{-2.0}$.

To enhance far distance predictions (>100 km) where generally a faster attenuation is observed, we utilized the G_5 filter. The GMPE with modified R_2 and additional far distance attenuation filter is called as "GK-09" and is shown in Fig. 2.

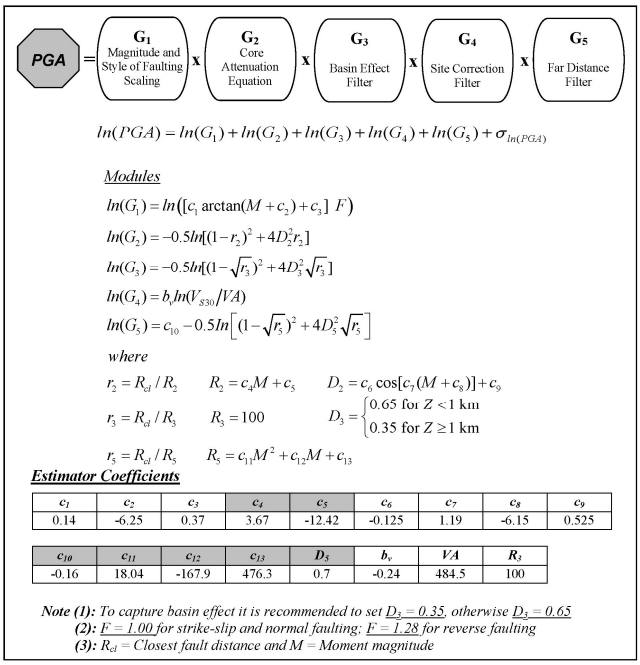

Figure 2. GK-09 global attenuation relation for free-field horizontal component.

Comparison of Predictions with Actual Data

The database is categorized into 9 magnitude bins having an interval of 0.4, and the GK-07 attenuation curve (without basin effect) is compared with actual data in each bin in Fig. 3. V_{S30} of predictions is taken as 400 m/sec as the average of the database. It is apparent that the GK-07 attenuation curve fits consistently well to actual data up to 100 km from the source indicating that our core equation is a good approximation of ground motion attenuation for a range of magnitudes. In order to achieve a better fit at intermediate distance range ($10<R<100$ km), corner distance parameter R_2 (R_0 in original equation in Graizer and Kalkan 2007) is modified. As opposed to its value computed for the extended NGA database, the Atlas database requires a slightly larger R_2 values (new c_4 and c_5 parameters are shown in Fig. 2).

The predictive power of the GK-09 is compared with the GK-07 and also with the actual recorded ground motion data in Fig. 3. Both GMPEs behave almost the same from 0 to 100 km of the fault, the difference (slightly higher predictions due to the GK-07 at near-field, and opposite at far-field) is associated with the first term, c_{10}, added to G_5 filter; without this scaling term both GMPEs would produce exactly same results up to 100 km. This scaling term helps to move slight distance bias in predictions. It is evident that G_5 filter in the GK-09 leads to visually enhanced predictions at both near- and far-field.

Fig. 3 also compares our predictions with one of the most commonly used NGA relations (Campbell and Bozorgnia 2008, CB-08). As compared to the CB-08, both GK-07 and GK-09 result in comparable predictions within 100 km and better predictions at larger distances for a range of magnitudes. The CB-08 consistently overestimates ground motion data at large distances ($R > 100$ km).

Residual Analysis and Standard Error

We computed the standard error (σ_{lnY} or simply σ) of prediction. σ of the GK-07 relation based on the NGA database is 0.55. For the Atlas database used in this paper the GK-07 and GK-09 yield larger σ as 0.85 and 0.83, respectively. Thus, the grey zones indicated in Fig. 3 bounded by 16- and 84 percentile (+/-σ) of the predictions are practically valid for both GMPEs. Most of the data falling in grey zone indicates reasonable predictions due to both GMPEs. Usually σ has a tendency to decrease when number of data points increases. An increase in σ is due to sparcity of the data in the Atlas database as opposed to well-constrained NGA database; the variability of PGA data in the Atlas database is much larger.

In addition to the total σ based on the entire database, the variation of σ within each magnitude bin is computed to examine the stability of the GMPEs at different magnitude levels. σ due to three GMPEs are marked in each panel in Fig. 3. σ demonstrates lower dependence on magnitude than observed by Strasser et al. (2009). As shown in Fig. 4, the GK-07 and GK-09 demonstrate similar level of standard error slightly lower than that of CB-08. Dependence of σ on distance is also examined by creating 25 distance bins with equal spacing of 20 km. Similar to magnitude, σ demonstrates relatively low dependence on distance; it decreases with increase in distance. It is possible to relate σ to magnitude and distance as:

$$\begin{aligned} \sigma(M) &= -0.043M + 1.10 \\ \sigma(R) &= -0.0004R + 0.89 \end{aligned} \tag{10}$$

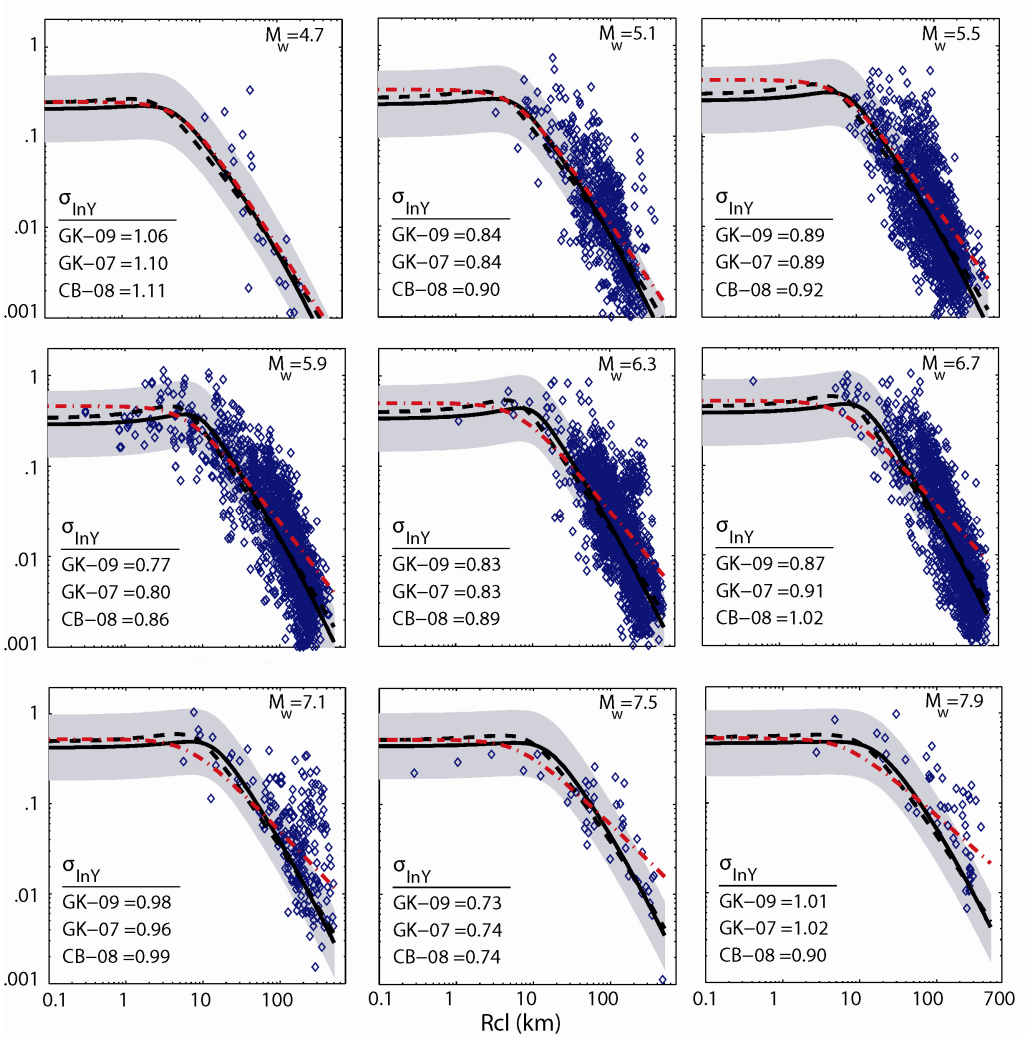

Figure 3. Comparison of GK-07 (dashed black line), GK-09 (solid black line) and CB-08 (dash dotted red line) GMPEs for $4.2 \leq M \leq 7.9$; data is divided into magnitude bins with an interval of 0.4; grey zones are bounded by $\pm\sigma$ of predictions.

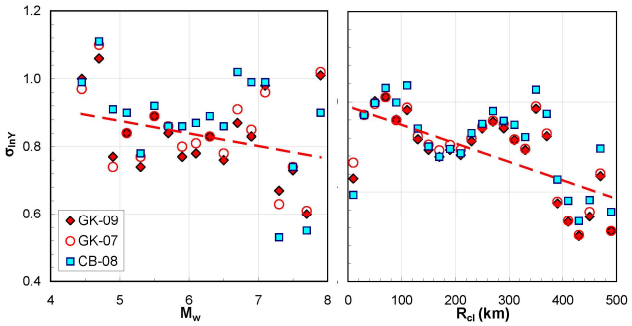

Figure 4. Variation of standard error of prediction with respect to M [left] and R_{cl} [right].

In order to investigate whether our predictions are biased against any independent parameter of estimations, residuals of predictions against magnitude, fault distance and V_{S30} are plotted in Fig. 5. The GK-07 shows a slight distance bias at far-field (over prediction), and no bias with

respect to magnitude and style of faulting. Note that the GK-07 is developed using data up to 200 km; the over prediction trend at far distances over 200 km is due to faster attenuation of low-amplitude data (such data is missing in the NGA database, see Fig. 1). Using an additional G_5 filter, we were able to eliminate this far-distance bias in the GK-09. Similar to the GK-07, GK-09 does not show any bias with respect to magnitude and style of faulting. These results indicate that the GK-09 can be used reliably for ground motion predictions for shallow crustal regions.

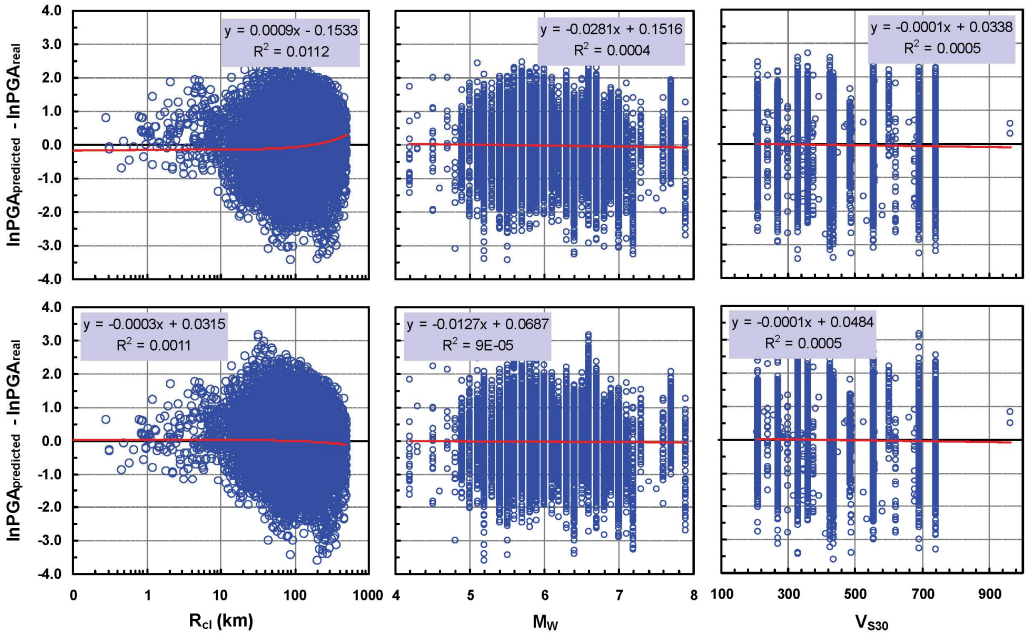

Figure 5. Distribution of residuals with respect to closest fault distance (R_{cl}), magnitude (M_W) and shear-wave velocity (V_{S30}) for GK-07 [top row]; and for GK-09 [bottom row].

Conclusions

In this paper, we tested the GK-07 using a large set of PGA data compiled from worldwide shallow crustal earthquakes. We observed that for distances more than 100 km from the fault, attenuation of ground motion demonstrates two main tendencies: Fast attenuation in the order of R^{-4}, and slow attenuation in the order of $R^{-1.5}$. For regions similar to the Central and Eastern U.S. with relatively high Q-values ground motion attenuation is about $R^{-1.5}$ at intermediate- and far-field, whereas for the Western U.S. with relatively low Q-values attenuation slope for distances of approximately more than 100 km is higher (almost R^{-4}). By calibrating two estimator coefficients in our original equation (GK-07) and implementing an additional far distance filter (G_5), we were able to obtain strong correlation between recorded data and predicted ones up to 500 km from the fault. The modified equation (GK-09) does not show any bias against distance, magnitude and V_{S30} measures. This demonstrates its reliability in predicting ground motions from shallow crustal events.

Standard error of the original GK-07 is 0.55 based on ~2000 data points; fitting the GK-09 to the Atlas database, which has seven times more data points, yields a standard error of 0.83, still less than the standard error of CB-08 ($\sigma_{CB\text{-}08}$=0.88) when it is fitted to the Atlas database. We found relatively weak dependence of standard error on magnitude and distance; the standard error tends to decrease with the increase in M_W and R_{cl}.

The filter-based modeling approach in ground motion prediction as presented for shallow crustal earthquakes can be used for other tectonic regions where subduction and intraplate events dominate the hazard. We expect a number of developed filters including the core filter G_2, the basin effect filter G_3 and the site correction filter G_4 to be applicable for different environments. For calculation of spectral acceleration (SA) response ordinates, the GK-09 presented here can be used together with our PGA-based predictive model for SA as described in Graizer and Kalkan (2009). The GK-07 and GK-09 GMPEs are available from the authors upon request.

Any opinions, findings and conclusions expressed in this paper are those of the authors and do not necessarily reflect the views of the U.S. Nuclear Regulatory Commission.

References

Abrahamson, N.A. and Silva, W.J. (2008). Summary of the Abrahamson and Silva NGA ground motion relations, *Earthquake Spectra*, **24**, No. 1, 67-98.

Boore, D. M., Joyner, W. B., and Fumal, T. E., 1997. Equations for estimating horizontal response spectra and peak acceleration from western North American earthquakes: a summary of recent work. *Seismol. Res. Lett.* **68**, 128-153.

Boore, D. M., and Atkinson, G. M., 2008. Ground motion prediction equations for the average horizontal component of PGA, PGV, and 5%-damped PSA at spectral periods between 0.01 s and 10.0 s, *Earthquake Spectra*, **24**, No. 1, 99-138.

Campbell, K. W., 1997. Empirical near-source attenuation relationships for horizontal and vertical components of peak ground acceleration, peak ground velocity, and pseudo-absolute acceleration response spectra. *Seismol. Res. Lett.* **68**, 154-179.

Campbell, K. W., 2003. Strong-motion attenuation relations, in *International Handbook of Earthquake andEngineering Seismology, Part B*, edited by W. H. K. Lee, H. Kanamori, P. C. Jennings, and C. Kisslinger, Academic Press, Burlington, Mass., 1003–1012.

Chiou, B., and Youngs, R., 2008. An NGA model for the average horizontal component of peak ground motion and response spectra, *Earthquake Spectra*, **24**, No. 1, 173-216.

Field, E. H., 2000. A modified ground motion attenuation relationship for Southern California that accounts for detailed site classification and a basin-depth effect. *Bull. Seism. Soc. Amer.,***90**, 209-221.

Graizer, V. and Kalkan, E., 2007. Ground Motion Attenuation Model for Peak Horizontal Acceleration from Shallow Crustal Earthquakes, *Earthquake Spectra*, **23**, No. 3, 585-613.

Graizer, V. and Kalkan, E., 2009. Prediction of response spectral acceleration ordinates based on PGA attenuation, *Earthquake Spectra*, **25**, No. 1, 39-69.

Idriss, I.M. (2008). An NGA empirical model for estimating the horizontal spectral values generated by shallow crustal earthquakes, *Earthquake Spectra*, **24**, No. 1.

Lee, V. W., Trifunac, M. D., Todorovska, M. I. and Novikova, E. I., 1995. Empirical equations describing attenuation of peak of strong ground motion, in terms of magnitude, distance, path effects and site conditions. Report No. CE 95-02. Los Angeles, California. 268 p.

Mitchell, B. J., and H. J. Hwang (1987). Effect of low Q sediments and crustal Q on Lg attenuation in the United States. *Bull. Seism. Soc. America*, **77**, No. 4, 1197-1210.

Power, M., Chiou, B., Abrahamson, N. and Roblee C., 2006. The next generation of ground motion attenuation models" (NGA) project: An overview. *In Proceedings, Eighth National Conference on Earthquake Engineering*, Paper No. 2022.

Singh, S. and R. B. Herrmann (1983). Regionalization of crustal coda Q in the continental United States, *J. Geophys. Res.,* **88**, 527-538.

Strasser F.O., Abrahamson N.E., and J.J. Bommer (2009). Sigma: Issues, Insights, and Challenges. *Seism. Res. Letters*, **80**, No.1, 40-56.